Influence of the Madden Julian Oscillation on precipitation and surface air temperature in South America

Mariano S. Alvarez, C. S. Vera, G. N. Kiladis & B. Liebmann

Climate Dynamics
Observational, Theoretical and Computational Research on the Climate System

ISSN 0930-7575

Clim Dyn
DOI 10.1007/s00382-015-2581-6

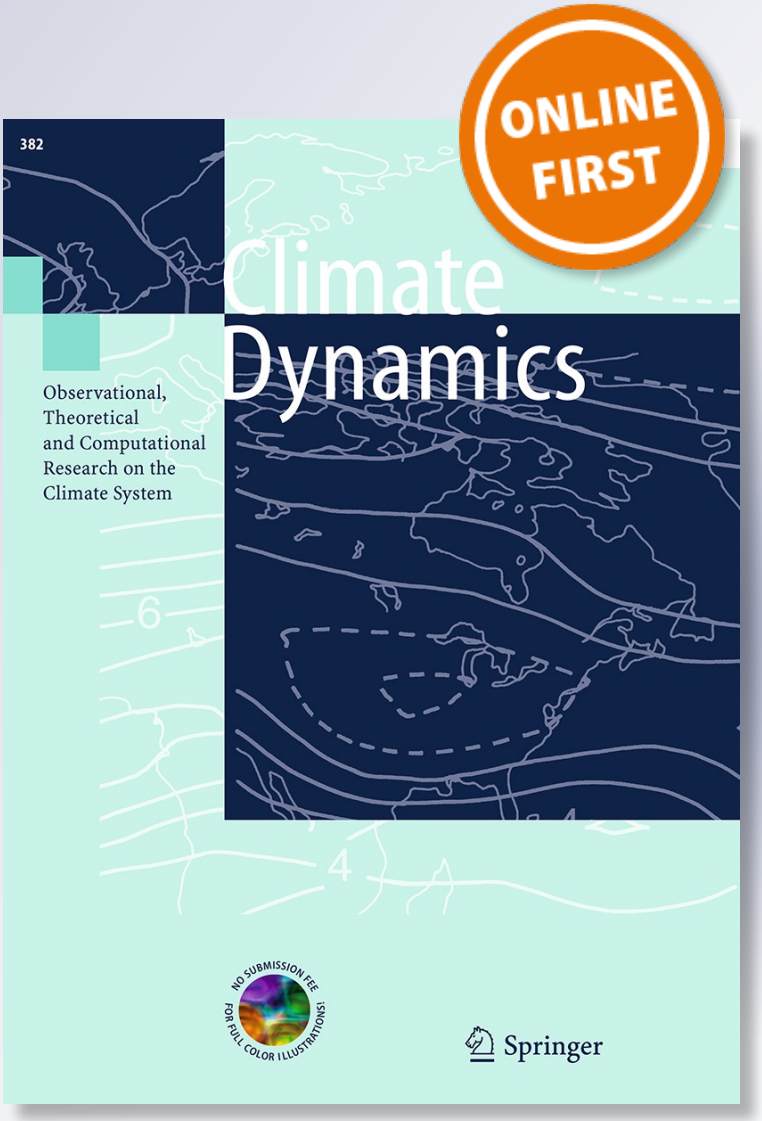

Springer

Clim Dyn
DOI 10.1007/s00382-015-2581-6

Influence of the Madden Julian Oscillation on precipitation and surface air temperature in South America

Mariano S. Alvarez[1] · C. S. Vera[1] · G. N. Kiladis[2] · B. Liebmann[2,3]

Received: 3 June 2014 / Accepted: 24 March 2015

Abstract The regional influence of the Madden–Julian oscillation (MJO) on South America is described. Maps of probability of weekly-averaged rainfall exceeding the upper tercile were computed for all seasons and related statistically with the phase of the MJO as characterized by the Wheeler–Hendon real-time multivariate MJO (RMM) index and with the OLR MJO Index. The accompanying surface air temperature and circulation anomalies were also calculated. The influence of the MJO on regional scales along with their marked seasonal variations was documented. During December–February when the South American monsoon system is active, chances of enhanced rainfall are observed in southeastern South America (SESA) region mainly during RMM phases 3 and 4, accompanied by cold anomalies in the extratropics, while enhanced rainfall in the South Atlantic Convergence Zone (SACZ) region is observed in phases 8 and 1. The SESA (SACZ) signal is characterized by upper-level convergence (divergence) over tropical South America and a cyclonic (anticyclonic) anomaly near the southern tip of the continent. Impacts during March–May are similar, but attenuated in the extratropics. Conversely, in June–November, reduced rainfall and cold anomalies are observed near the coast of the SACZ region during phases 4 and 5, favored by upper-level convergence over tropical South America and an anticyclonic anomaly over southern South America. In September–November, enhanced rainfall and upper-level divergence are observed in the SACZ region during phases 7 and 8. These signals are generated primarily through the propagation of Rossby wave energy generated in the region of anomalous heating associated with the MJO.

Keywords Madden–Julian oscillation · South America · Precipitation · Surface air temperature · Impacts

1 Introduction

During the last decade it has been increasingly recognized that climate information, if it could be provided weeks in advance, would be extremely important for decision making within many socio-economic sectors. Such information relies on the monitoring and prediction of the intraseasonal (IS) variability and in particular of the Madden–Julian oscillation (MJO). MJO impacts have been assessed globally (e.g., Donald et al. 2006) and regionally for different parts of the world, such as for the United States (Zhou et al. 2012; Jones et al. 2011), Chile (Barret et al. 2012), the Caribbean (Martin and Schumacher 2011), Australia (Wheeler et al. 2009), Southeast China (Zhang et al. 2009), India (Pai et al. 2009), Mexico and Central America (Barlow and Salstein 2006) and East Africa (Pohl and Camberlin 2006), and in many other regions (see Lau and Waliser 2012).

Precipitation in South America exhibits considerable variability on IS timescales in all seasons (e.g., Liebmann et al. 1999 for austral summer and Alvarez et al. 2014 for austral winter). During summer, Nogues-Paegle and Mo (1997) detected a dipole in the IS variability of convection, a pattern that shows centers of action of opposite signs

✉ Mariano S. Alvarez
alvarez@cima.fcen.uba.ar

[1] Centro de Investigaciones del Mar y la Atmósfera, (CIMA/CONICET-UBA), DCAO/FCEN, UMI-IFAECI/CNRS, Buenos Aires, Argentina

[2] Earth System Research Laboratory, NOAA, Boulder, CO, USA

[3] Cooperative Institute for Research in Environmental Sciences, University of Colorado, Boulder, CO, USA

Published online: 03 April 2015

between the South American convergence zone (SACZ) and southeastern South America (SESA). The MJO influence in South America has been identified in both austral summer precipitation (e.g., Liebmann et al. 2004; Jones et al. 2004; De Souza and Ambrizzi 2006) and in the occurrence of extreme wet and dry events (e.g., Muza et al. 2009). A large modulation of precipitation by the MJO in the area of the SACZ has been found (e.g., Paegle et al. 2000; Carvalho et al. 2004). Furthermore, large IS variability has also been recorded in surface air temperature anomalies in southern South America (e.g., Cerne and Vera 2011), which seems to be at least partially influenced by MJO activity (Naumann and Vargas 2010).

Nevertheless, detailed knowledge of the MJO influence on South America climate is still quite incomplete. A more detailed description of the influence of the MJO on rainfall, temperature and circulation as well as its seasonal variations would provide a fundamental basis for MJO monitoring in the region. This work is inspired by the study of Wheeler et al. (2009), who quantified the MJO influence on precipitation in Australia. This has allowed operational monitoring of that influence by the Australian Bureau of Meteorology (http://www.bom.gov.au/climate/mjo/).

The aim of this work is to provide a quantitative analysis of the variability of both precipitation and temperature explained by the MJO in South America, and a discussion of the large-scale circulation anomalies that account for that influence. The study covers the entire seasonal cycle, as both regional climate and MJO activity have a strong seasonality. The paper is organized as follows. Section 2 describes the data and methodology used; Sect. 3 describes the seasonal evolution of regional climate anomalies in South America associated with MJO activity as well as the associated large-scale circulation anomalies; and conclusions are presented in Sect. 4.

2 Data and methodology

2.1 Data

Daily values of 250-hPa geopotential heights, 0.21-sigma level velocity potential, and surface air temperature were taken from the National Center for Environmental Prediction-National Center for Atmospheric Research (NCEP-NCAR) reanalysis dataset (Kalnay et al. 1996), from December 1979 to November 2012. These datasets are on a 2.5° × 2.5° grid. Daily precipitation on a 1° × 1° grid is from the dataset developed by Liebmann and Allured (2005), within the period December 1979 to November 2011.

Wheeler and Hendon (2004) constructed the real-time multivariate (RMM) index to monitor MJO evolution. They used the two leading empirical orthogonal functions (EOFs) of the combined fields of normalized 850-hPa zonal wind, 200-hPa zonal wind and outgoing longwave radiation (OLR) data averaged from 15°S to 15°N. The RMM index is defined from the two principal component time series, with RMM1 associated with EOF1 and RMM2 with EOF2. The index is used to describe the temporal evolution of the amplitude and phase of the MJO and is divided into eight phases, according to the region in which convection is enhanced. The same EOF pair is used for the entire year, and despite strong seasonality in the latitude of convection, during all seasons in phases 8 and 1 convection is maximum in the western hemisphere and Africa, phases 2 and 3 correspond to a maximum over the Indian Ocean, phases 4 and 5 peak over the Maritime Continent, and phases 6 and 7 over the western Pacific (Wheeler and Hendon 2004). It has been shown that statistical prediction of the RMM index has useful skill out to 2 weeks by using RMM1 and RMM2 as predictors at an initial time (Maharaj and Wheeler 2005).

The analysis presented here was repeated with an OLR only based MJO index (OMI) derived by Kiladis et al. (2014). This index is based on the first two EOFs of "MJO-filtered" OLR, calculated daily using a sliding 121 day window to take into account the seasonal migration of the MJO OLR activity. Since RMM is dominated by the circulation component of the MJO (Straub 2013), there can be substantial differences between the amplitude and phase of the OMI and RMM for individual MJO events, although differences are less pronounced for statistical results using either index (Kiladis et al. 2014). Results for this study were quite similar using either index, so we focus on the results for RMM for consistency with Wheeler et al. (2009). A brief discussion and some examples of the RMM–OMI comparison can be found in the "Appendix".

2.2 Methodology

All calculations were done separately for the 3-month seasons December–February (DJF), March–May (MAM), June–August (JJA) and September–November (SON). Daily anomalies of temperature, geopotential height and velocity potential were calculated at every grid point by subtracting the long-term average for that day so as to remove the seasonal cycle.

Following Zhou et al. (2011), composites of temperature, geopotential height and velocity potential anomalies were generated for each MJO phase through regression modeling. The advantage of the regression-based approach is that it fits the regression model to observations from all phases (without reducing the dataset length). The linear model presented by Zhou et al. (2011) was used in this study, to quantify the linear response (E) of a given

atmospheric variable to the MJO at a certain location. At every grid point a linear regression is then computed using RMM1 and RMM2 (hereafter x_1 and x_2) as predictors, obtaining two regression constants, β_1 and β_2; that is

$$E = \beta_1 x_1 + \beta_2 x_2$$

which can be written as:

$$E = \gamma_1 A \cos(\theta - \gamma_2)$$

where $\gamma_1 = \sqrt{\beta_1^2 + \beta_2^2}$ scales the instantaneous amplitude of the MJO ($A = \sqrt{x_1^2 + x_2^2}$) and $\gamma_2 = \tan^{-1}(\beta_2/\beta_1)$ shifts its phase $\theta = \tan^{-1}(x_2/x_1)$.

It is possible to estimate for every grid point and for a given phase the expected response in order to generate composites using a fixed amplitude, which was set in this study to its mean value, while varying x_1 and x_2 to define the phase according to the phase-space defined by x_1 and x_2. For example, θ in MJO phase 5 was set to $\pi/8$, in MJO phase 6 to $3\pi/8$ and so on, adding $\pi/4$ for the next phase in a counter-clockwise direction. Since all phases are used to fit the regression, a sinusoidally varying model is produced, so, for example, MJO phases 5 and 1 are the exact opposites, as their phases are shifted by π.

Two maps can be constructed to describe the composites: a map of γ_1, that shows the amplitude of the response E to a complete cycle of the MJO, and a map of γ_2, that shows the phase at which E is maximum. These maps are known as coamplitude and cophase maps. If the instantaneous amplitude of the MJO is smaller than 1, then it is considered a neutral MJO day. Statistical significance of the composites was tested as in Zhou et al. (2011), who used Monte Carlo techniques to create an approximated sampling distribution of the coefficient of determination, assuming that the dependent variable is not related to the independent variables (x_1 and x_2).

Composites for rainfall were computed following Wheeler et al. (2009), although they explored additional rainfall metrics than the present study. Wheeler et al. (2009) computed daily anomalies and the probability of 7-day running mean rainfall exceeding different thresholds: the upper tercile, the highest decile and 1 mm day^{-1}. Wheeler et al. (2009) concluded that the probability of exceeding the weekly tercile was the most appropriate metric, as they are less influenced by outliers than daily anomalies, and occur more frequently than highest decile events, therefore achieving greater statistical confidence in the results. Furthermore, as the upper-tercile threshold fluctuates with location and season, it is more appropriate than a constant metric. Hence, the upper tercile was the metric chosen for this study.

The tercile exceedences were computed from 7-day running mean precipitation. For each phase the number of days in which weekly rainfall was above the upper tercile (67th percentile) was counted and divided by the total number of days in each phase to obtain the probability of exceeding the threshold. Therefore, the probability composites for each phase show the chance that precipitation has exceeded the upper tercile at a given location during that phase. The composites are scaled by the local mean probability of exceeding the threshold, which is nominally 33 %. Statistical significance was tested following the nonparametric re-sampling approach proposed by Wheeler et al. (2009), which consists of generating 400 synthetic realizations of the probability composites, obtained by successively shifting the time sequence of the observed MJO phases relative to the rainfall time series, to create the null distribution with which to compare the composite.

3 Results

3.1 Large-scale dynamics

The influence of the MJO on circulation anomalies in the vicinity of South America can be exerted mainly by two different ways: (1) changes in the tropical circulation associated to the eastward passage of MJO diabatic heating anomalies along the equator; and (2) changes in the extratropical circulation anomalies through Rossby wave trains extending between tropical western Pacific-Indian Ocean sector and South America (Berbery and Nogues-Paegle 1993; Mo and Higgins 1998; Kiladis and Mo 1998; Revell et al. 2001). During austral summer, changes in the divergent tropical circulation can enhance or inhibit convection associated with the South American monsoon system (SAMS), mainly within the SACZ, which in turn impacts the vertical motion in the subtropics. At the same time, regional circulation anomalies mainly over southern South America can be influenced by the large-scale extratropical circulation anomalies in turn induced by the convection enhanced or suppressed by the MJO over tropical western Pacific-Indian tropical oceans. While these two mechanisms have been highlighted in previous works focused on summer (e.g., Carvalho et al. 2004; Liebmann et al. 2004), neither their combined influence over South America nor their seasonality have been explored in detail.

The following sub-sections focus on the circulation anomalies associated to MJO that can help to explain the MJO signals of both rainfall and temperature anomalies identified in South America. Composites of large-scale anomalies of geopotential height at 250 hPa and velocity potential at 0.21 sigma-level are analyzed as the key features associated with the extratropical and tropical circulation changes, respectively. They are presented in Figs. 1, 2, 3 and 4 for each season and for MJO phases 1–4, which, with the opposite sign, are to be interpreted as MJO phases

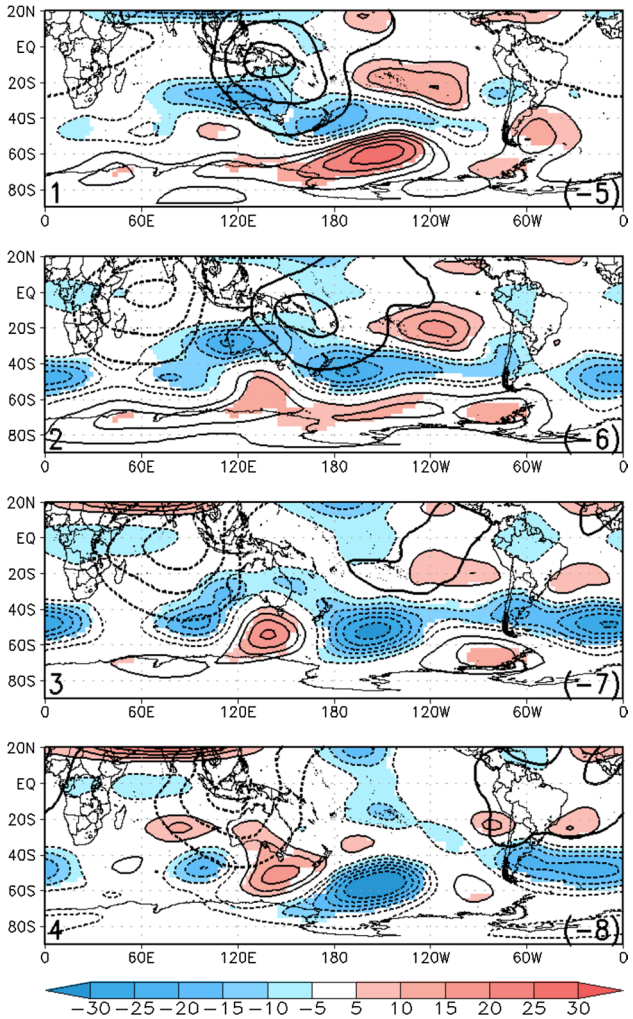

Fig. 1 Composites of DJF 250 hPa geopotential height anomalies (*shaded* and *contours*) and 0.21 sigma-level velocity potential (*thick contours*) according to RMM index-defined MJO phases *1–4* (expressed on the *bottom left* of *each panel*) obtained with the regression model. The composites for MJO phases *5–8* are identical but with the sign reversed (expressed on the *bottom right* of *each panel*, see Sect. 2.2). Only 95 % significant values are *shaded* for the geopotential height anomalies. *Contour* interval is 5 gpm and 0 *contour* is omitted. Velocity potential *contour* interval is 1×10^7 m^2 s^{-1} and the first *contour* is 2×10^7 m^2 s^{-1}; *negative contours* are *dashed*

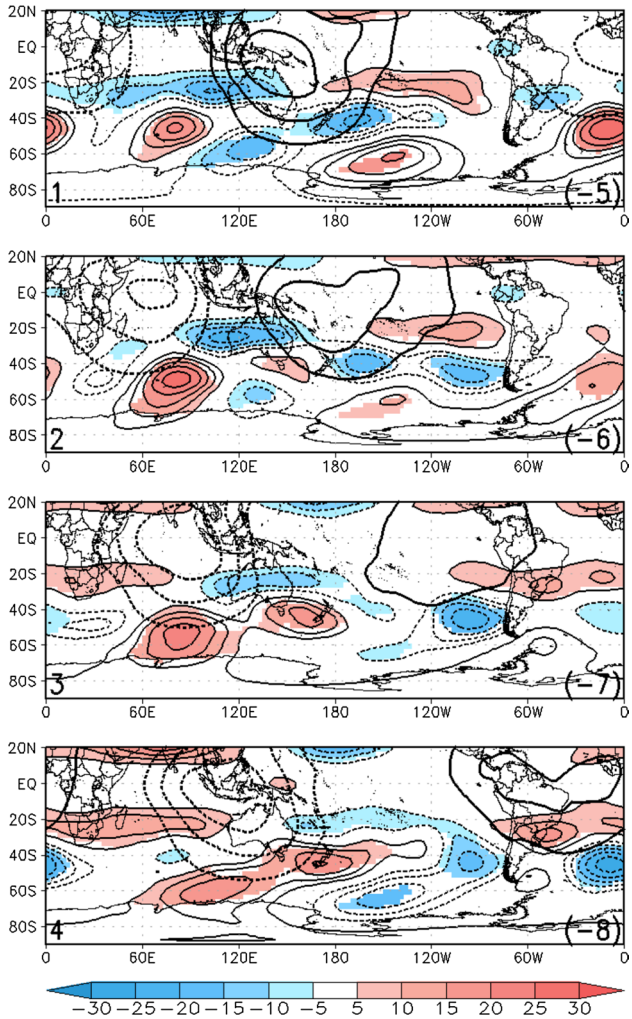

Fig. 2 As in Fig. 1 but for MAM

5–8. Note that the eastward MJO propagation, depicted by the upper-level velocity potential anomalies along the tropics (Figs. 1, 2, 3, 4), represents the mean evolution of the oscillation. Individual MJO events may not have such coherent behavior.

3.1.1 December–February

Anomalous upper-level tropical convergence (represented by positive velocity potential anomalies) progresses eastwards from western tropical Pacific during phase 1 and arrives in tropical South America by phases 4 and 5 (Fig. 1), inhibiting upward motion in that region. At the same time, between phases 2 and 5, a Rossby wave train develops between Australia and the Bellinghausen—Amudsen Seas and is refracted equatorward, resulting in an extratropical cyclonic anomaly over subtropical South America. Its development promotes anomalous upward motion over SESA and subsidence in the SACZ region.

On the other hand, from phases 6 to 1, anomalous upper-level tropical divergence (indicated by negative velocity potential anomalies) progresses from the western tropical Pacific and reaches tropical South America by phase 8 (Fig. 1) where it favors anomalous upward motion through phase 1 and consequently inhibits upward motion in the corresponding subtropics due to compensatory subsidence. In addition, through phases 6–1, a Rossby wave train extends between Indian-western Pacific tropical oceans and South America, which contributes to the development of an anticyclonic anomaly in the southern tip of the continent

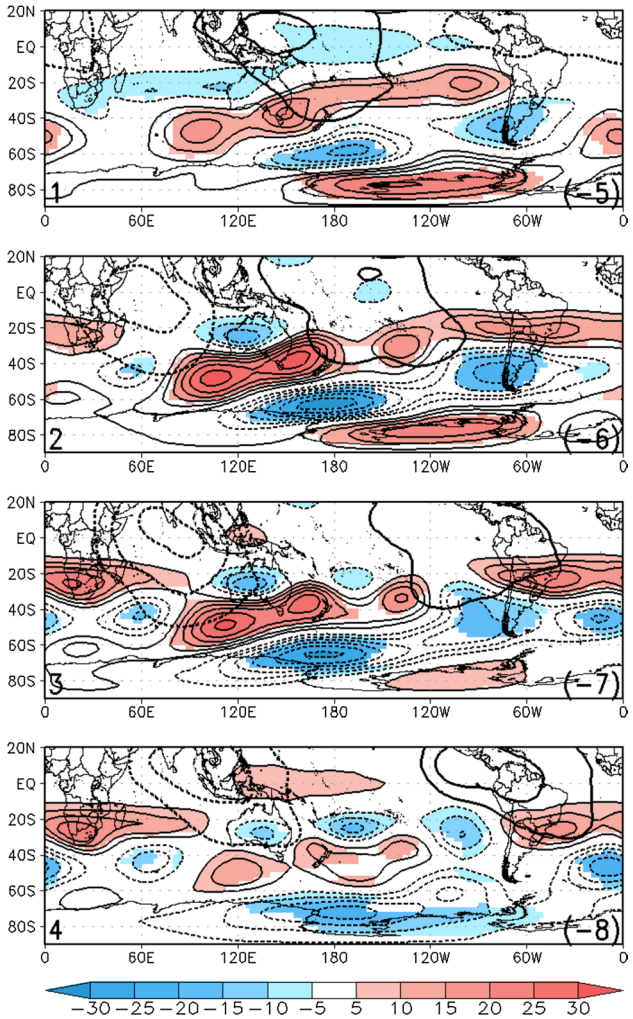

Fig. 3 As in Fig. 1 but for JJA

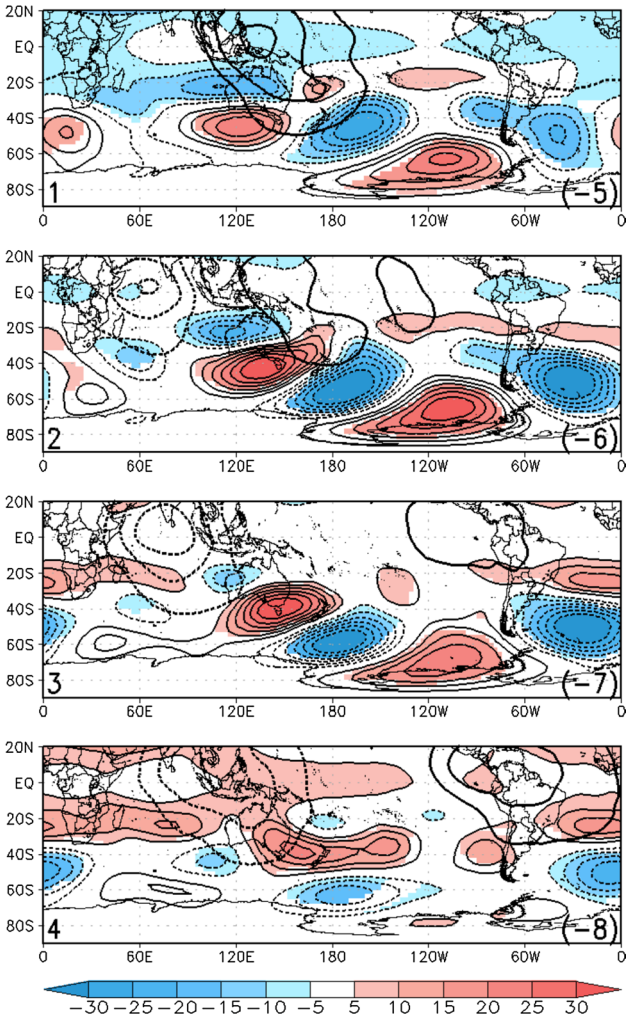

Fig. 4 As in Fig. 1 but for SON

that also favors subsidence in the subtropics and extratropics of South America.

3.1.2 March–May

The tropical divergent circulation anomalies in MAM (Fig. 2) are similar to those observed in summer (Fig. 1), inhibiting upward motion over tropical South America mainly between phases 4 and 5 and favoring it mainly between phases 8 and 1 (Fig. 2). During this season, however, the extratropical Rossby wave train, which emerges from the anomalous equatorial convection in the equatorial Indian Ocean (Fig. 2, phases 3–5 and 7–2), propagates poleward farther to the west than in summer. This results in less influence of the rotational circulation anomalies over the continent. As a consequence, the associated cyclonic circulation anomaly is over the southeastern Pacific (Fig. 2, phases 2–4), whereas during summer it was centered over the tip of the continent (Fig. 1, phases 1–4). This feature therefore contributes less to inducing anomalous upward motion in SESA. The opposite happens with the Rossby wave train observed between phases 6 and 1, which is related to an anticyclonic circulation anomaly located over the southeastern Pacific, farther to the west than in summer.

3.1.3 June–August

During winter, significant changes are observed in the behavior of the extratropical Rossby wave train as compared to that observed in summer and fall. The Rossby wavetrain emerging from the Indian Ocean observed in winter is associated with a more zonally oriented circulation anomaly pattern with a lower planetary wave number that extends more towards the Antarctic coast, closer to the Antarctic Peninsula (Fig. 3). Furthermore, a zonally oriented Rossby wave train is discernible mainly between phases 3 and 4 (and with opposite sign between phases 7 and 8) in the subtropical latitudes of the South Pacific,

likely favored by the presence of the winter mean subtropical jet. Such combination of wave trains evolving at both subtropical and subpolar latitudes of the South Pacific has also been identified in previous works of austral winter IS variability (e.g., Alvarez et al. 2014). Between phases 2 and 4 (6 and 8), an anticyclonic (cyclonic) anomaly in subtropical South America and cyclonic (anticyclonic) one further south are evident.

Regarding the divergent circulation, upper-level divergence is observed over the continent during MJO phases 8 and 1, favoring ascent in the region, while the opposite is found when upper-level convergence anomalies associated with MJO cross the continent mainly between phases 4 and 5 (Fig. 3). In particular, the features observed between phases 2 and 3 agree broadly with that identified by Alvarez et al. (2014) in association with the wet phase of the activity of the leading pattern of rainfall variability on IS timescales, which is characterized by a spatial monopole extended over tropical South America.

3.1.4 September–November

During this trimester the rainy season onset occurs on average in tropical South America and both SAMS and SACZ related convection develops (e.g., Vera et al. 2006). Moreover, tropical divergent circulation anomalies associated with MJO activity (Fig. 4) evolve quite similarly to those observed in DJF (Fig. 1). During phases 7–1 (4–5) upper-level divergence (convergence) is evident over tropical South America, promoting chances of upward (downward) motion over the SAMS-SACZ region (Fig. 4). On the other hand, the mean extratropical circulation in the South Pacific during this season shares some similarities to that observed in winter (Fig. 3). In particular, the Rossby wave train associated to MJO activity is very well defined and coherent along the high-latitude South Pacific, except that it exhibits an equatorward bend at around 110ºW compared to the pattern in winter (Fig. 3). Consequently, this refraction and the equatorward propagation are mainly along the southwestern Atlantic Ocean, influencing the circulation anomalies in the continent to a lower degree.

3.1.5 Coamplitude and cophase

The characteristics of the large-scale circulation anomalies described above are summarized in Fig. 5, which shows for each season the maps of coamplitude (defined in Sect. 2) for 250-hPa geopotential height anomalies associated with MJO activity. In DJF, the signal extends from Australia southeastward to Bellinghausen—Amundsen seas and refracts equatorward over South America, with the largest amplitude to the north of Ross Sea. In MAM, the signal is much weaker in general and the pattern seems to be

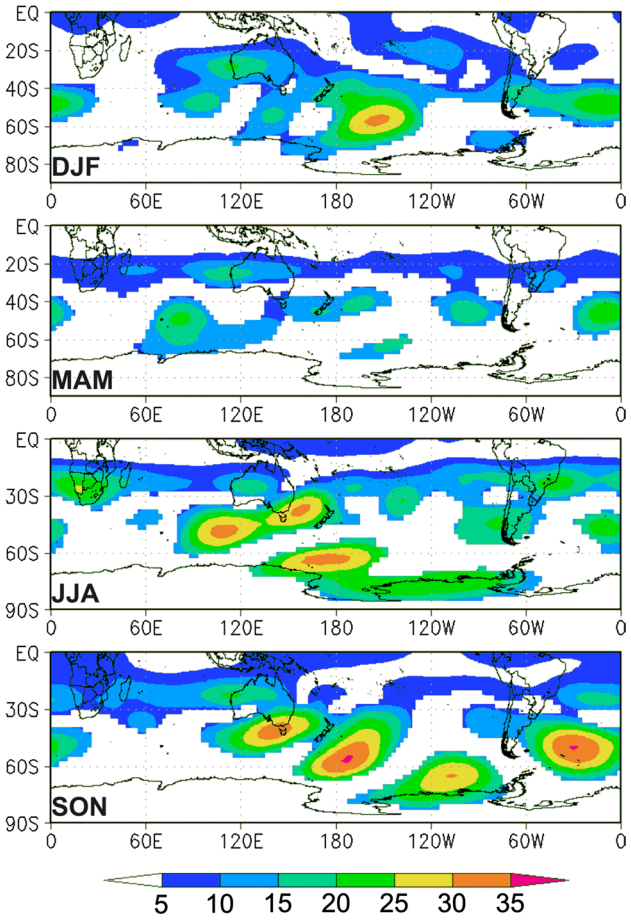

Fig. 5 Coamplitude maps of 250 hPa geopotential height anomaly for each season

refracted at higher latitudes and farther west than in DJF, so the influence over South America is less evident. In JJA, the signal has increased, it is very coherent, and it seems to be associated with a lower planetary wave number than in the previous season. During this season, the signal is refracted near the Antarctic coast and at a longitude closer to the Antarctic Peninsula. A zonally oriented Rossby wave train of moderate amplitude along the subtropical latitudes of the South Pacific is also evident. In SON the Rossby wave train arching between Australia and the South Atlantic has the largest amplitude among all seasons and it is also very coherent. It refracts equatorward at the same longitude than in winter but at lower latitude, while the signal continues to be very large and coherent well into the South Atlantic Ocean. On the other hand, no signal associated with subtropical wave trains is discernible in this season.

Figure 6 shows the cophase (defined in Sect. 2) of the 250-hPa negative-geopotential height anomalies associated with MJO activity. Each color defines the phase at which the cyclonic anomaly of geopotential height is most intense at a certain location. In the subtropics from the Indian

Ocean to South America, the phase increases smoothly at all seasons, indicating the eastward-propagating MJO signal in the circulation. Within the extratropics, there is evidence of the signal propagating along an arch between mainly Indian Ocean–Australia sector and South America–South Atlantic sector but with large seasonal variation. In DJF, there is a dominant cyclonic signal at the SACZ oceanic portion location on phases 7–8–1, while further south it is during phases 3–4. In MAM, the most evident signal over South America is within the tropical regions during phases 7–8, while there is no signal at the southern tip of the continent. On the other hand, in JJA the cyclonic signal goes from central South America during phase 7 to both equatorward and poleward in phases 8–1 and even in phase 2 in Patagonia. In SON, while both the subtropical and northern portion of South America exhibit significant signal between phases 1 and 2, in the SACZ region this is present in phases 7 and 8.

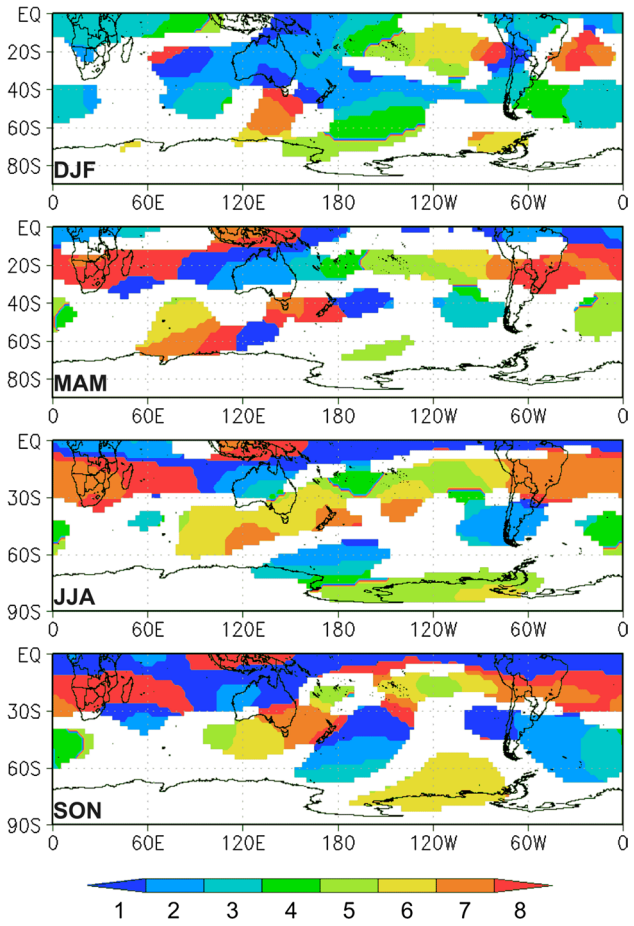

Fig. 6 Cophase maps of negative 250 hPa geopotential height anomaly for each season. *Each color* defines one of the 8 RMM phases of the MJO

Overall, the results of this subsection substantiate the fact that in the mean, MJO heating initiates Rossby wave energy propagation into the South Pacific sector, some of which refracts equatorward over the South American sector, with the amount varying by season. At the same time, the tropical portion of the MJO dynamical signal also induces circulation anomalies over tropical South America that would either favor or disfavor convective activity. We now examine the impacts of these circulations on the surface variability over South America.

3.2 Daily temperature composites

Daily temperature anomalies were composited according to a mean-amplitude MJO, for each MJO phase, and by season. During DJF (Fig. 7), warm anomalies are present over the extratropical part of the continent from phase 6 to 1, when anomalous downward (upward) motion is favored over the SESA (SACZ) region (Fig. 1). This is in agreement with the mechanism described by previous works (e.g., Cerne et al.

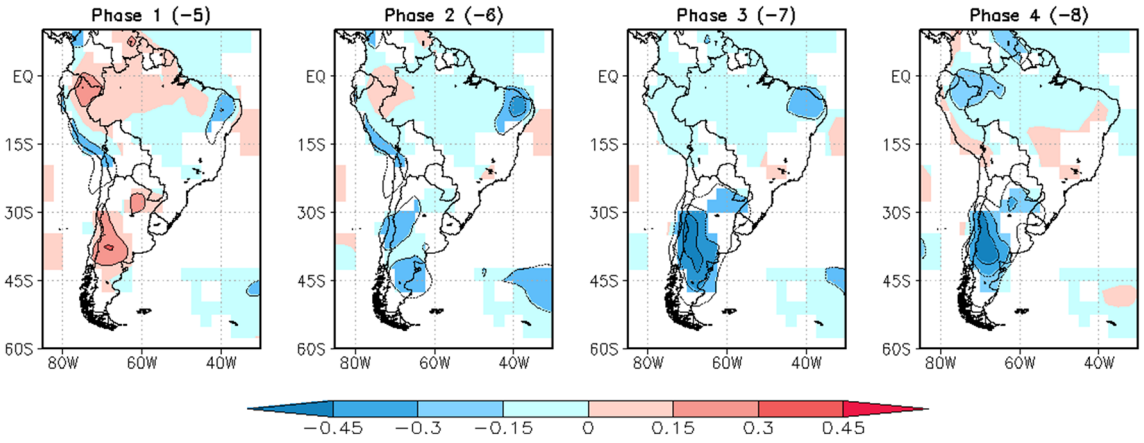

Fig. 7 Composites of DJF surface air temperature anomalies according to RMM index-defined MJO phase *1–4* obtained with the regression model. The composites for MJO phases *5–8* are identical but with the sign reversed, and those are indicated between *parentheses* (see Sect. 2.2). Only 95 % significant values are shown. *Contour* interval is 0.15 °C and 0 *contour* is omitted

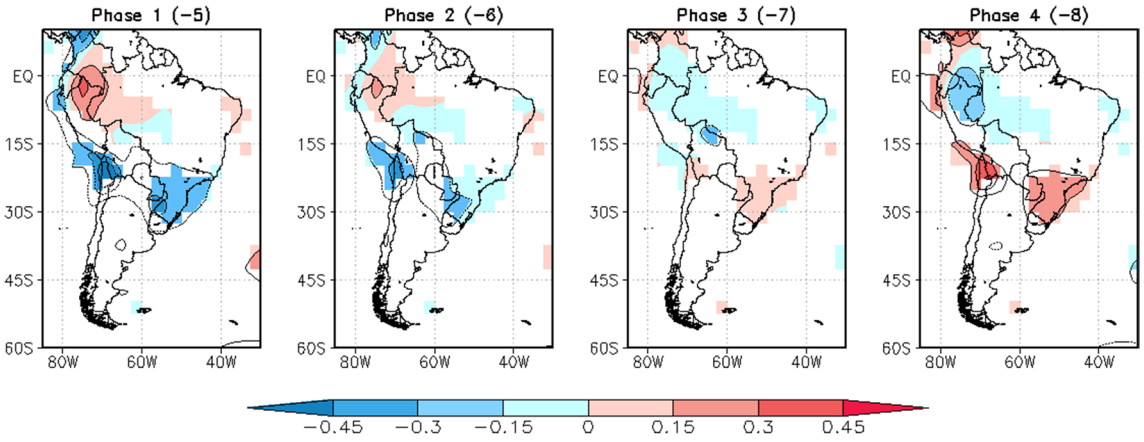

Fig. 8 As in Fig. 7 but for MAM

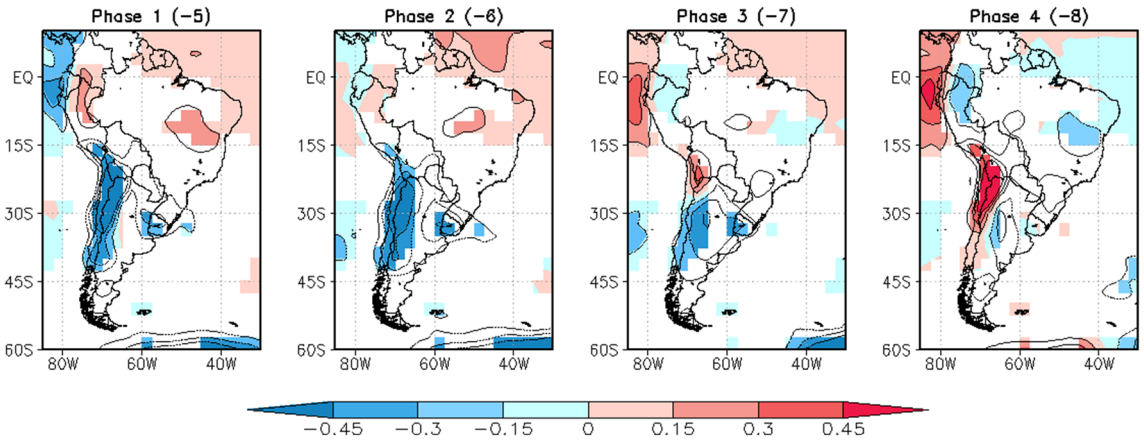

Fig. 9 As in Fig. 7 but for JJA

2007): compensatory subsidence over subtropical South America, clear skies and diabatic warming are promoted during enhanced convection over the SACZ region. On the other hand, cold anomalies are more intense over extratropical South America from phases 2 to 5. We note that the vertical structure of the extratropical anomalies isolated in this study is nearly equivalent barotropic, with only a slight southwestward tilt with height (not shown), as was found in previous studies (e.g., Liebmann et al. 2004). Thus the cold anomalies over extratropical South America in these phases can be related to cold advection and the anomalous upward motion promoted in turn by the cyclonic anomaly observed over this region (Fig. 1). Temperature anomalies are large over northern Patagonia, central-western Argentina and central Chile. Northeastern Brazil also shows cold (warm) anomalies in phases 1–3 (5–7).

In MAM (Fig. 8), cold (warm) anomalies are stronger mainly over northern Chile, western Bolivia, eastern Paraguay and southern Brazil from phases 8 to 2 (4–6), when anomalous upward (downward) motion is favored due to the cyclonic (anticyclonic) anomaly observed in the region. Meanwhile, warm (cold) anomalies are observed within northwest South America. Throughout JJA (Fig. 9) significant cold (warm) anomalies are observed in phase 8 (4) over northern Chile and extending to the south and west in phases 1–3 (5–6), which can be associated with the cyclonic (anticyclonic) anomaly located in southern South America (Fig. 3).

In SON (Fig. 10), warm anomalies extend from central Chile and central-western Argentina towards northwestern Argentina and Paraguay from phases 6 to 8, explained both by warm advection from the north and also partially by compensatory subsidence conditions promoted by the upper-level divergence located over tropical South America (Fig. 4). The latter is similar to the mechanism described during summer. The southwestern Atlantic Ocean also shows significant warm anomalies during these phases, and in phase 8 cold anomalies start to develop over the

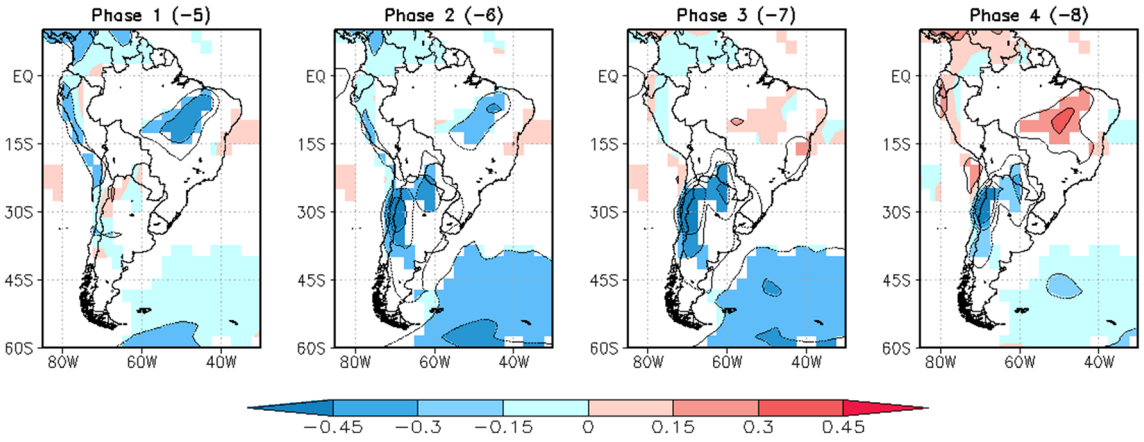

Fig. 10 As in Fig. 7 but for SON

continental SACZ region, which are evident until phase 2. On the other hand, the subtropical regions of the continent exhibit cold anomalies from phases 2 to 4, as does the southwestern Atlantic Ocean, which is the result of cold advection between the large anticyclone over the Amundsen Sea in combination with the strong South Atlantic cyclone in Fig. 4. From phases 4 to 6 warm anomalies are observed over the SACZ region, a signal at least in part due to the tropical subsidence induced by upper level convergence.

3.3 Weekly rainfall probability

In this section we discuss changes in South American precipitation variations associated with the MJO. As discussed above, these are quantified in terms of the probability of precipitation exceeding the upper tercile. The probabilities are scaled such that a greater (less) than 1.0 ratio of probabilities would mean an increased (reduced) chance of above-threshold precipitation during a certain phase of the MJO. As an example, a ratio of 1.5 (0.5) would mean that the chance of exceeding the threshold was increased (reduced) by 50 %. As the nominal probability of exceeding the upper tercile is 33 %, a ratio of 1.5 (0.5) during a certain phase means that there is a 49.5 % (16.5 %) of probability of exceeding the threshold during that phase. Maps of the mean seasonal rainfall, the value of the event threshold and the composite for the neutral MJO cases are also shown for reference. Changes in precipitation are related with those identified in the circulation anomalies at large and regional scales (Figs. 1, 2, 3, 4). Such analysis provides some indications of the mechanisms explaining the MJO impact on the precipitation. A more detailed study of the dynamic and thermodynamic processes involved is beyond the scope of the present work.

During DJF (Fig. 11), there is an increased probability of above-threshold precipitation in eastern Brazil during phase 1, which disappears in phase 2 except along the northern coast. During phases 3 and 4 there are ratios in excess of 1.6 over SESA, as well as lower than 1.0 ratios in the continental portion of the SACZ, a pattern of summer variability that resembles the dipole first described by Nogues-Paegle and Mo (1997). This can be related to anomalous upward motion over SESA promoted by the cyclonic anomaly observed over extratropical South America (Fig. 1). Furthermore, during phase 4 there is an increased chance of exceeding the threshold in central eastern Argentina. Centered on phase 5, but also distinguishable in phases 4 and 6, there is a dramatic decrease in probabilities over most of eastern Brazil, including the climatological SACZ region, with the ratios lower than 0.4 in some regions. The reduced probabilities are associated with the anomalous upper-level tropical convergence that produces subsidence, consistent with positive velocity potential anomalies in Fig. 1. In MJO phase 8, central and eastern Brazil shows regions of ratios in excess of 1.2, in association with upper-level divergence over that region (Fig. 1).

During neutral MJO conditions (lower-right panel of Fig. 11), the probability of exceeding the threshold in the position of the climatological SACZ (in SESA) is slightly above (below) 1.0 ratio, and there is no other large region with a marked influence of MJO. Furthermore, the SACZ and SESA have been previously identified as having large IS variability also on timescales closer to 20 days (e.g., Gonzalez and Vera 2013), associated with alternating centers of enhanced and suppressed precipitation between those two regions (e.g., Paegle et al. 2000).

In MAM (Fig. 12), during phase 2 and to a lesser extent in phases 1 and 3, much of eastern Brazil exhibits elevated probabilities, though the large scale circulation might be able to explain this only during phase 1, given

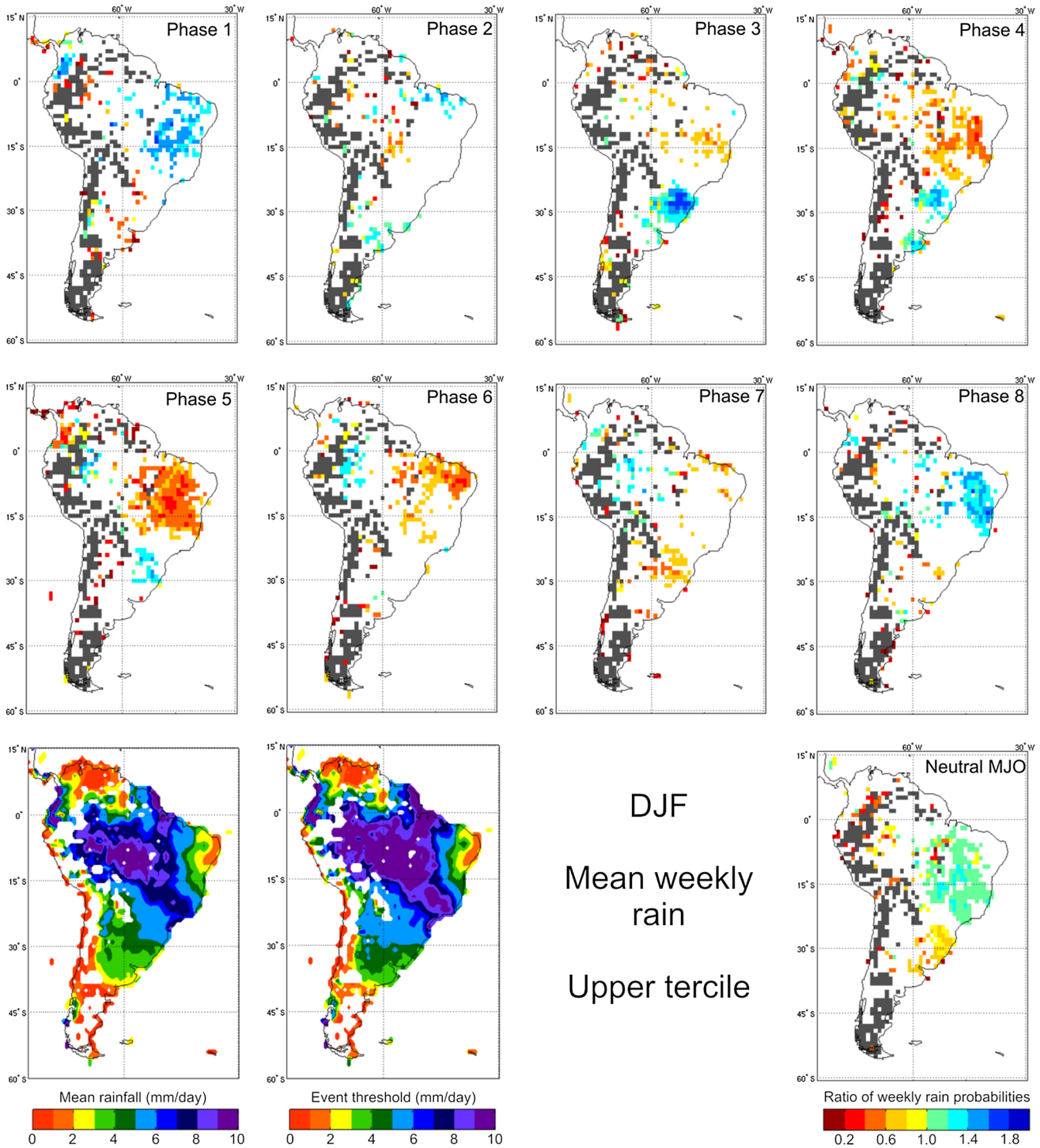

Fig. 11 DJF season (*top* and *middle rows*) composites of weekly rainfall probabilities for RMM index-defined MJO phases *1–8*. The probabilities refer to the chance of weekly averaged rainfall exceeding the upper tercile, expressed as a ratio with the mean probability (nominally 33 %) for every grid point. Only 10 % significant values are shown and those gridpoints with missing values were masked out in *grey* (*bottom right*). Composite of weekly rainfall probabilities for neutral MJO cases (*bottom left*). Climatological DJF mean weekly rainfall in South America (*bottom middle*). Weekly rainfall threshold

that upper-level divergence is observed over tropical South America as well as a cyclonic anomaly over SESA (Fig. 2). An area of eastern Brazil with ratios below 1 appears in phase 4, and continues to expand through phase 6, when low ratios are prevalent over most of eastern Brazil. At the same time ratios above 1.0 are observed in SESA, although

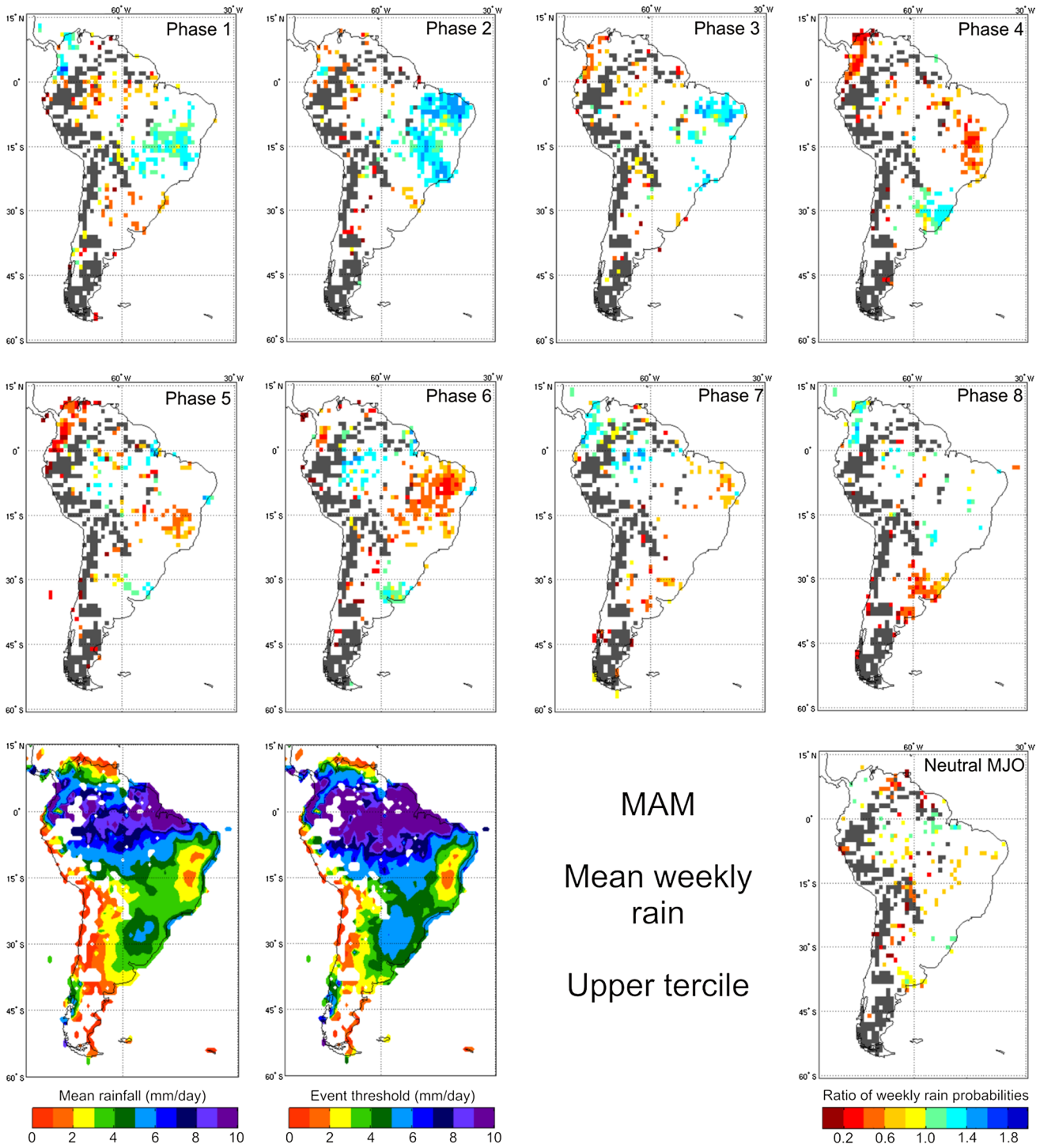

Fig. 12 As in Fig. 11 but for MAM

the associated circulation anomaly pattern is not clear. This area switches to below 1.0 by phase 8. During other phases and neutral conditions, only scattered areas of abnormal probabilities are evident.

JJA is the dry season throughout tropical South America and there are fewer areas of coherent ratios than in the other seasons. During phases 8 and 1, however, greater chances of enhanced rainfall are observed in northern South America (Fig. 13) in association with the passage across the continent of the upper-level divergence anomalies associated with MJO (Fig. 3). The opposite is found when the upper-level convergence anomalies associated with MJO cross the

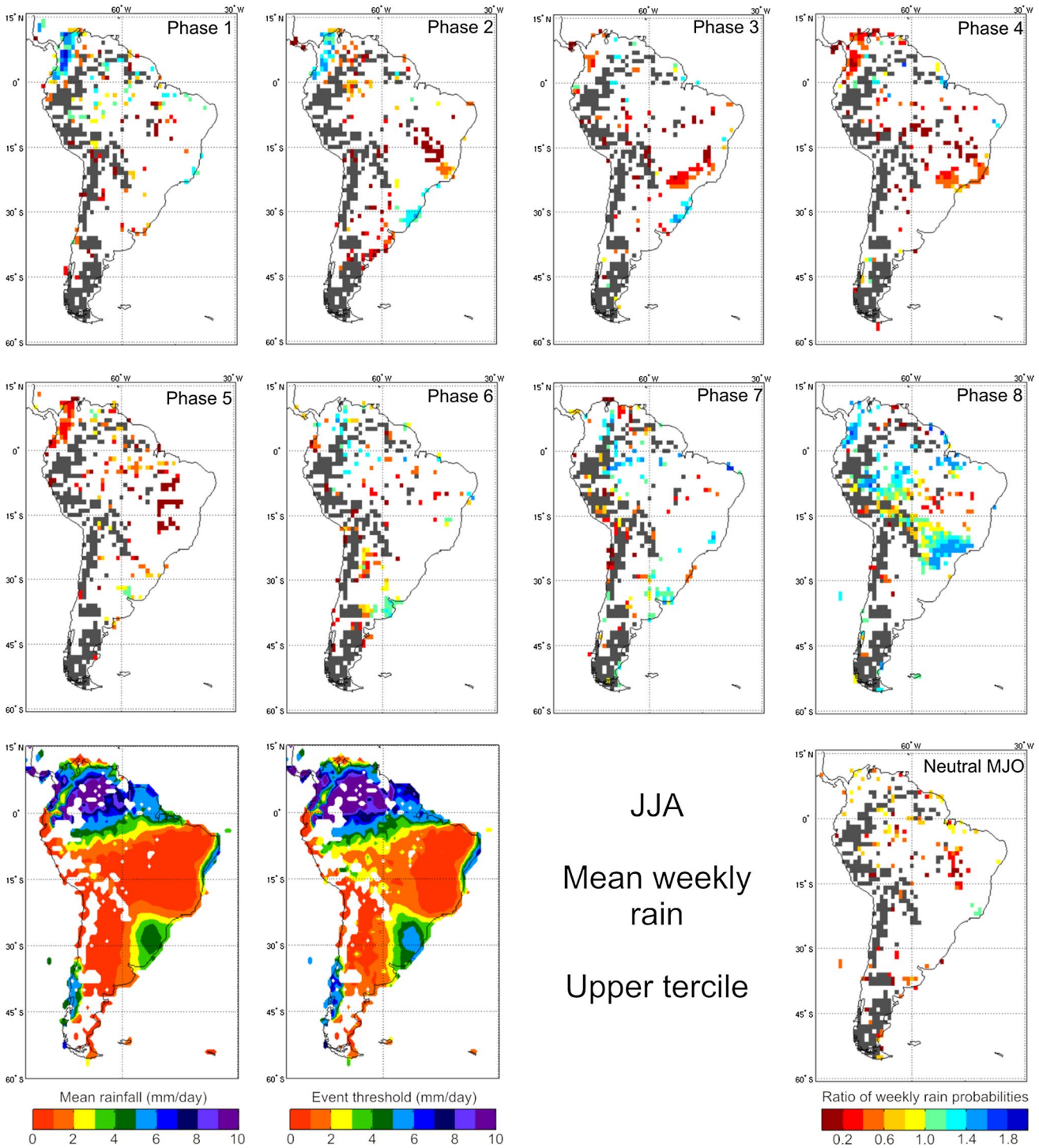

Fig. 13 As in Fig. 11 but for JJA

continent mainly between phases 4 and 5. The far northwest of the continent seems to be particularly responsive to these circulation changes, as there is an increased probability of enhanced rainfall in phases 8, 1 and 2, a probability which turns to lower than nominal during phases 4 and 5. MJO phase 8 also shows excess ratios in southeastern Brazil (Fig. 13). The regional circulation configuration may explain this, as during phase 8 a cyclonic anomaly is observed in eastern subtropical South America, which would force upward motion over the region (Fig. 3).

SON (Fig. 14) shares characteristics with both summer and winter. During phases 4 and 5 ratios are smaller

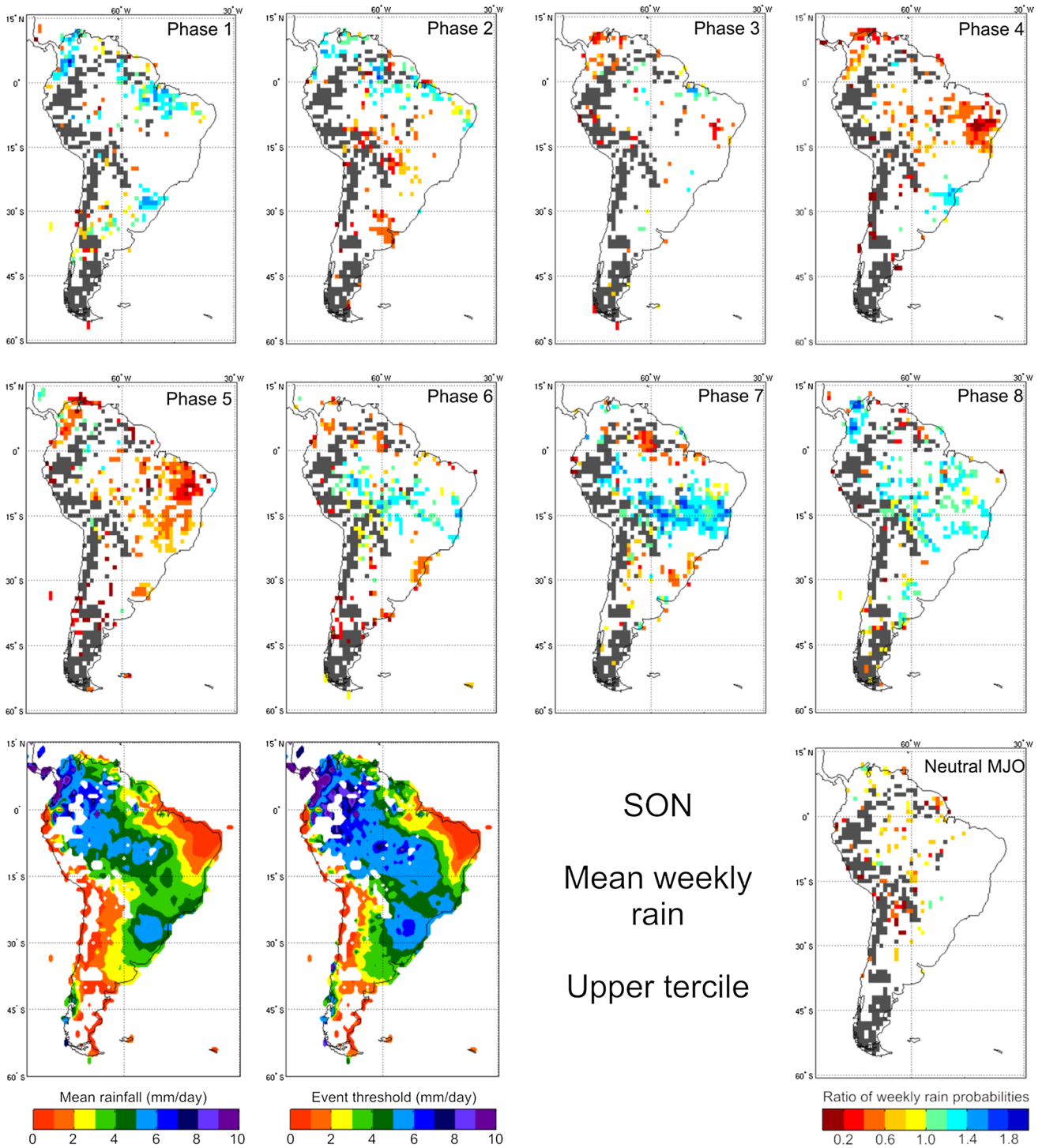

Fig. 14 As in Fig. 11 but for SON

than 1.0 in eastern Brazil, but they are weaker than those observed in DJF. The prominent dipole of the summer, present to a lesser extent in MAM, is distinctly missing in SON. On the other hand, during phase 7 enhanced ratios are observed in the region of Brazil centered at 15°S. Similar to JJA, a cyclonic anomaly centered at around 20°S (Fig. 4) enhances upward motion, which would promote enhanced rainfall over this region. On the contrary, the opposite flow configuration between phases 3 and 5 (Fig. 4) would reduce the chances of enhanced rainfall.

Further south, the cyclonic anomaly that evolves from west of the Antarctic Peninsula in phase 7, to subtropical

South America on phase 1 (Fig. 4) appears to develop favorable conditions for enhanced precipitation over SESA during that phase. Accordingly, the anticyclonic anomaly located over southern South America during phases 6 and 7 seems to reduce chances of enhanced rainfall over SESA (Fig. 14). During neutral MJO conditions the pattern of ratios is mostly scattered.

4 Conclusions

The impact of the MJO on precipitation and surface air temperature over South America was analyzed, providing a reference about the timing and intensity of MJO signal over this continent that can be used for monitoring and prediction activities in the region. The precipitation changes associated with MJO activity were quantified following Wheeler et al. (2009), in probabilistic terms of the probability of exceeding the upper tercile of the weekly-averaged rainfall distribution. In addition, the anomalies of surface air temperature in South America and large-scale upper-level circulation in the Southern Hemisphere were described using the linear regression model proposed by Zhou et al. (2011). The signals were obtained with respect to the Wheeler and Hendon (2004) RMM index, and were found to be robust for the most part when using the OLR-only derived index of Kiladis et al. (2014) as shown in the "Appendix".

MJO influence on regional climate in South America was detected in all seasons, but with large seasonal variations. In DJF, when the SAMS is active, increased chances of precipitation exceeding the upper tercile are observed in the SESA (SACZ) regions mainly between phases 3 and 4 (8 and 1). Such a pattern is favored by upper-level convergence (divergence) over tropical South America and a cyclonic (anticyclonic) anomaly around its southern tip, both being circulation responses to MJO activity. During MAM, the impacts are somewhat similar to those observed in DJF except that the extratropical Rossby wave train influences extratropical South America to a lower degree. On the other hand, in JJA and SON, during the dry season in the tropics, reduced chances of rainfall exceeding the upper tercile are observed in SACZ mainly between phases 4 and 5, favored by upper-level convergence over tropical South America and an anticyclonic anomaly located further south, both being circulation responses to MJO activity.

Results suggest that the SAMS activity induces a large modulation on the MJO influence on climate variability in South America. It is also evident that in all seasons circulation anomalies over South America that in turn induce both precipitation and surface air temperature anomalies are a combination between the divergent circulation response to MJO with largest amplitude at the tropics and the rotational circulation response to MJO, with largest amplitude at the extratropics. However, the controlling mechanisms of the circulation response, such as timing and signal location over both South America and the South Pacific Ocean, require further investigation. Therefore, an improved understanding of the tropical–extratropical processes associated with the MJO signal propagation over the South Pacific from the Indian Ocean–Australia sector towards South America–South Atlantic sector will be the purpose of a future study.

Acknowledgments This research was supported by UBACyT 20020100100434, ANPCyT PICT-2010-2110. M.S.A. is supported by a Ph.D. grant from CONICET, Argentina.

Appendix

The phase of the OMI was made directly comparable to RMM Index following Kiladis et al. (2014), and the calculations in this work were then repeated using that index. As the RMM Index is constructed using OLR and circulation, it was expected for the RMM composites to show more signal overall, particularly in the geopotential height anomalies composites. As an example, Figs. 15 and 16 show the large-scale anomalies of geopotential height at 250 hPa and velocity potential at 0.21 sigma-level and for MJO phases 1–4, which, with the opposite sign, are to be interpreted as MJO phases 5–8, for DJF and SON respectively.

The OMI-based (Fig. 15) and the RMM index-based (Fig. 1) composites for the DJF season are remarkably similar. The extent of the statistically significant signals and the amplitude of the anomalies are generally reduced, although the locations of the centers agree well. The OMI-based composites for MAM and JJA (not shown) also resulted comparable to the RMM index-based, though some centers over the southern Indian Ocean presented larger amplitude when using the OMI during MAM. During JJA, significance spans slightly larger regions using RMM index, and is particularly strong to the southwest of South America on phases 1 and 2 (and 5 and 6, Fig. 3), which was not the case when using OMI.

Table 2 of Kiladis et al. (2014) shows that the OMI leads the RMM Index by 4 days in SON, being the greatest lag of the four seasons. It was therefore expected that we would find the greatest differences in the composites during SON. Figure 16 shows that phases 2, 3 and 4 of the OMI-based composites may be associated to phases 1, 2 and 3 of the RMM Index-based composites respectively (Fig. 4), consistent with the lag between the indexes. The OMI-based composites (Fig. 16) did not show a significant signal to the southwest of South America, and significance and amplitude of the centers were reduced compared to RMM index-based composites (Fig. 4).

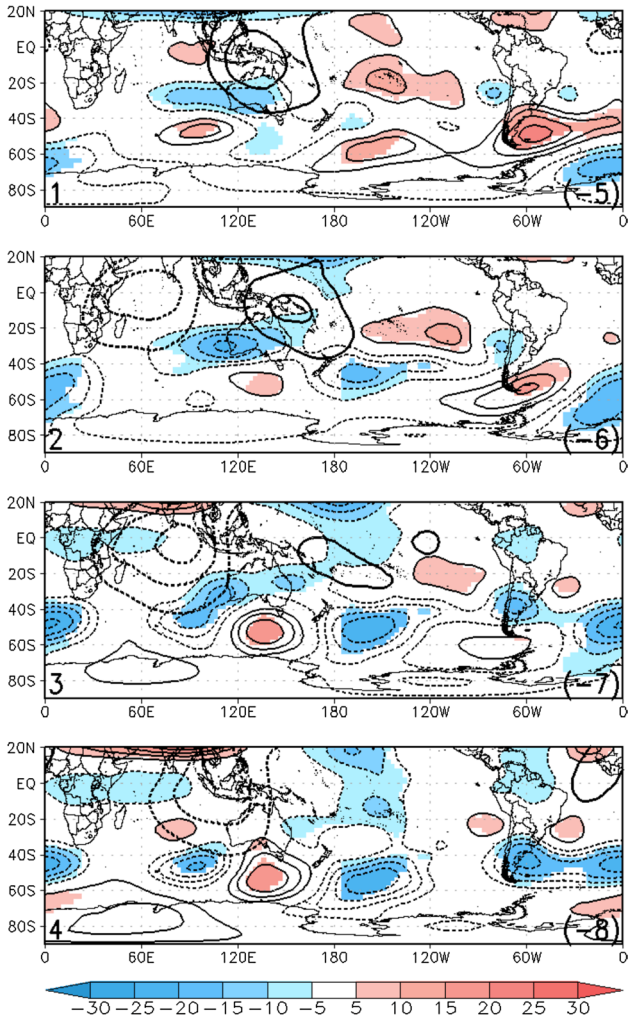

Fig. 15 As in Fig. 1 but using the OMI to generate the composite

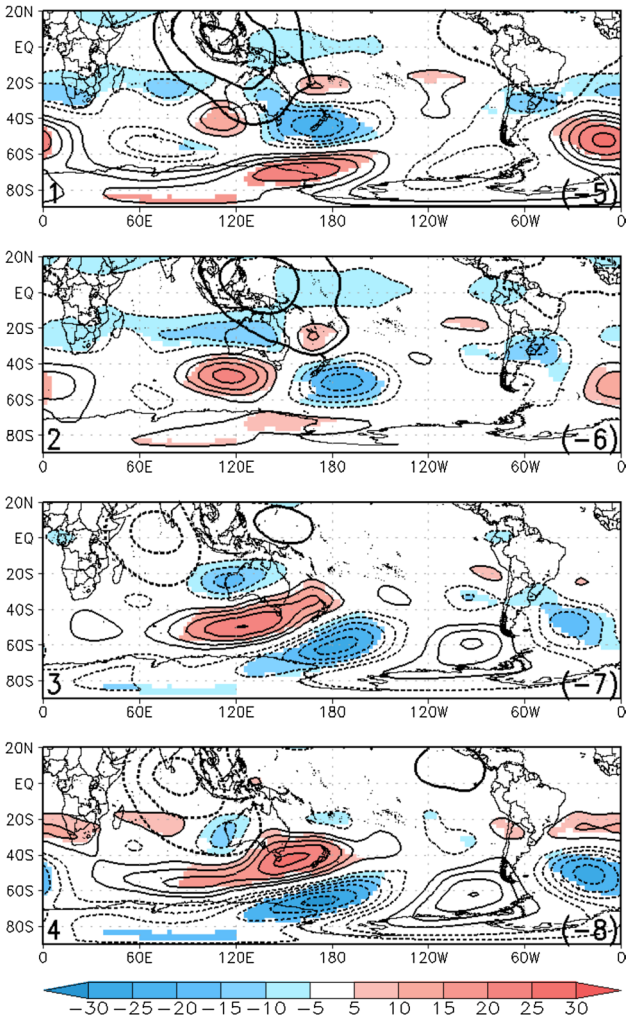

Fig. 16 As in Fig. 4 but using the OMI to generate the composite

Figures 17 and 18 show the rainfall probability composites for DJF and SON respectively, analogous to Figs. 11 and 14 but using the OMI as opposed to the RMM index. Again, during DJF both composites results are quite alike (Figs. 11, 17), although the OMI-based probability composites seem to have significant signal over more regions of South America, with a few exceptions, as eastern Brazil in MJO phase 8 and during neutral MJO cases, when OMI-based composites do not show a coherent signal (Fig. 17). During MAM, the OMI-based composites (not shown) are overall similar to RMM index-based ones, however, the most remarkable discrepancies are that the former showed a stronger signal with ratios lower than 1.0 over SESA (eastern Argentina) on MJO phase 1 (3) and greater than 1.0 ratios over SESA and west of the South Brazilian Bight on MJO phase 8. During JJA, OMI-based composites are seen to have an overall larger signal (not shown), though these signals are, as in RMM-based composites, less coherent than in the other seasons.

As previously seen with the circulation composites, during SON, OMI-based rainfall probability composites (Fig. 18) lead RMM index-based ones (Fig. 14) by one MJO-phase, that is, OMI-based composite on MJO phase 1 resembles the RMM index-based composite during MJO phase 8, and so on. The most remarkable differences when comparing both composites were observed over eastern Argentina and SESA, though the general pattern resulted similar.

The OMI-based temperature composites (not shown) presented overall less regions with statistically significant signal. The regional pattern observed in DJF was quite similar to the RMM index-based composites (Fig. 7), the latter presenting higher values over northern Patagonia. During MAM, RMM index-based composites showed significance over SESA and slightly higher anomalies over the continent compared to the OMI-based composites, while during JJA the extratropical significant signal using OMI was considerably reduced. Finally, during SON, the

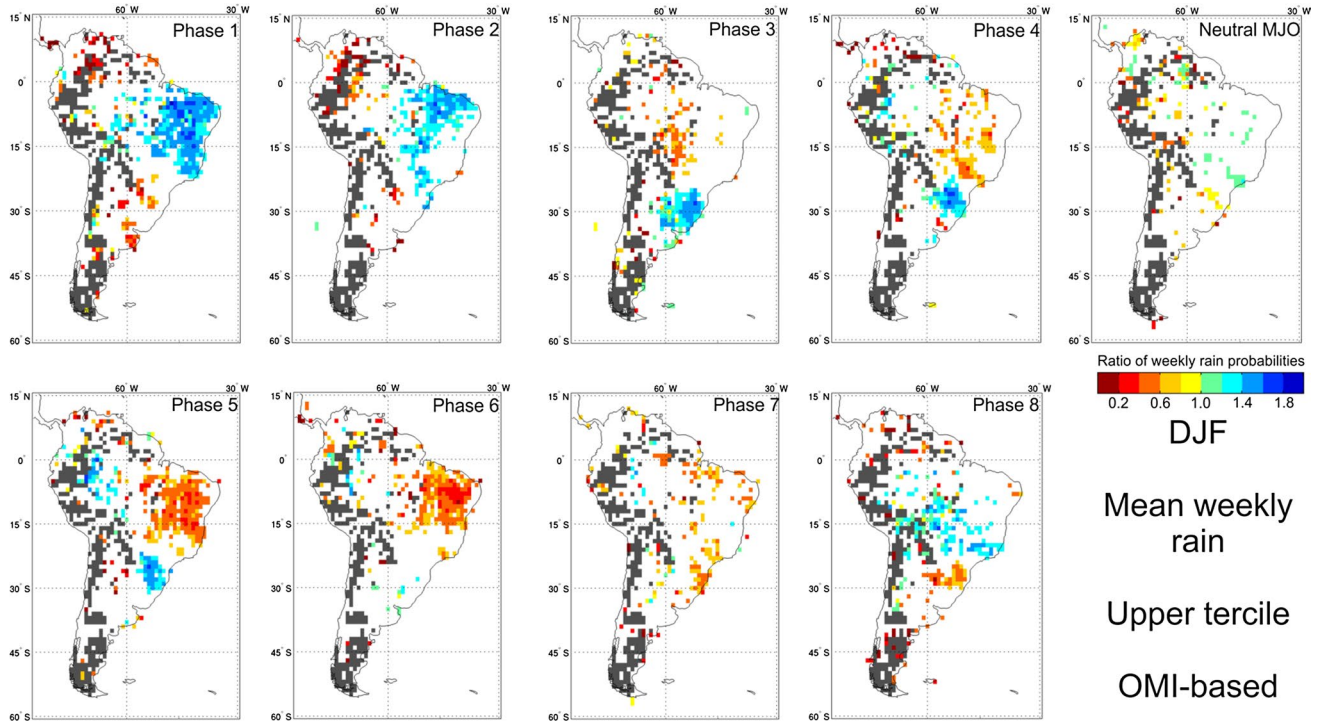

Fig. 17 DJF season composites of weekly rainfall probabilities for OMI-defined MJO phases *1–8* and neutral MJO cases. The probabilities refer to the chance of weekly averaged rainfall exceeding the upper tercile, expressed as a ratio with the mean probability (nominally 33 %) for every grid point. Only 10 % significant values are shown and those gridpoints with missing values were masked out in *grey*

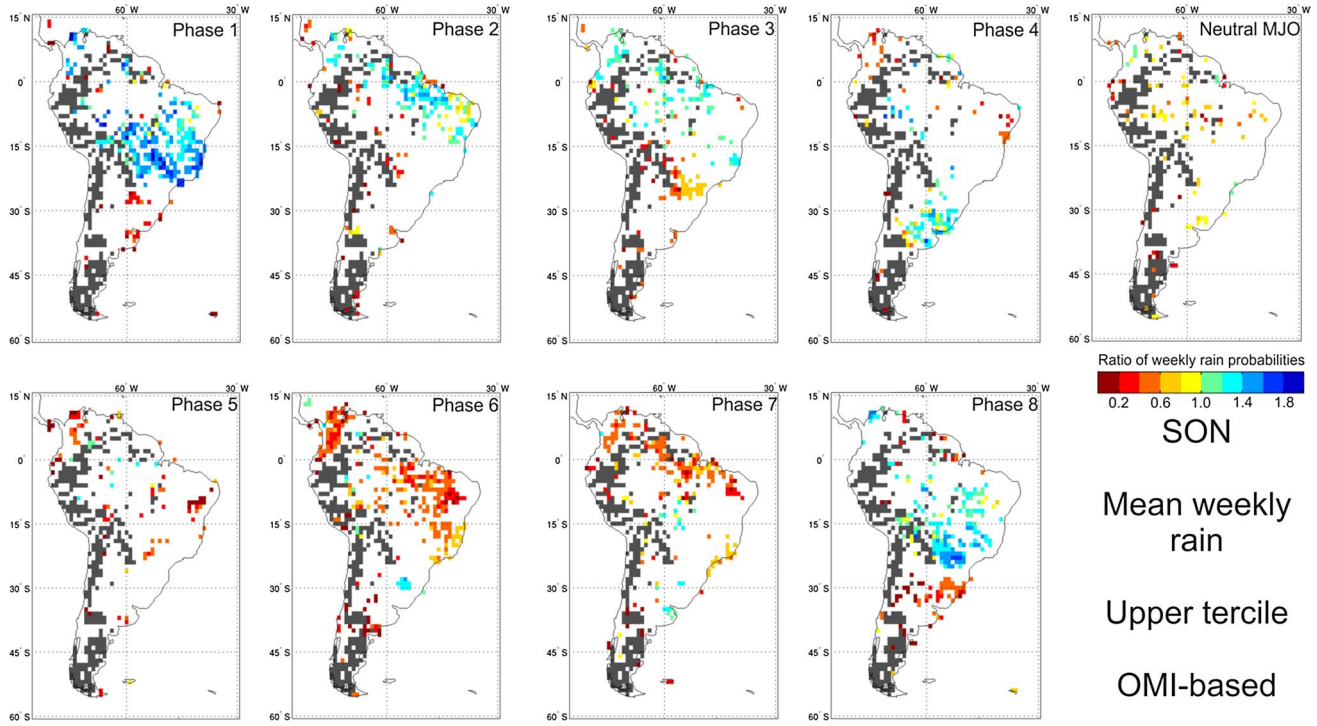

Fig. 18 As in Fig. 17 but for SON

lag observed in the comparison with the other variables was also present in temperature composites. In particular, the signal over northwestern Argentina and in the South Atlantic Ocean was noticeably reduced when the OMI was used. The fact that OMI signals are comparable to those using RMM is reassuring, although it is perhaps not surprising that in some cases there is less significance to the OMI results, since a significant portion of the RMM signal is likely related to circulation anomalies over the South America sector (Straub 2013; Kiladis et al. 2014).

References

Alvarez MS, Vera CS, Kiladis GN, Liebmann B (2014) Intraseasonal variability in South America during the cold season. Clim Dyn 42(11–12):3253–3269. doi:10.1007/s00382-013-1872-z

Barlow M, Salstein D (2006) Summertime influence of the Madden–Julian oscillation on daily rainfall over Mexico and Central America. Geophys Res Lett 33:L21708. doi:10.1029/2006GL027738

Barret BS, Carrasco JF, Testino AP (2012) Madden–Julian oscillation (MJO) modulation of atmospheric circulation and Chilean winter precipitation. J Clim 25(5):1678–1688

Berbery EH, Nogues-Paegle J (1993) Intraseasonal interactions between the tropics and extratropics in the Southern Hemisphere. J Atmos Sci 50(13):1950–1965

Carvalho LMV, Jones C, Liebmann B (2004) The South Atlantic convergence zone: intensity, form, persistence, relationships with intraseasonal to interannual activity and extreme rainfall. J Clim 17:88–108

Cerne B, Vera C (2011) Influence of the intraseasonal variability on heat waves in subtropical South America. Clim Dyn 36:2265–2277

Cerne B, Vera CS, Liebmann B (2007) The nature of a heat wave in eastern Argentina occurring during SALLJEX. Mon Weather Rev 135:1165–1174

De Souza EB, Ambrizzi T (2006) Modulation of the intraseasonal rainfall over tropical Brazil by the Madden–Julian oscillation. Int J Clim 26(13):1759–1776

Donald A, Meinke H, Power B, deMaia AHN, Wheeler MC, White N, Stone RC, Ribbe J (2006) Near-global impact of the Madden–Julian oscillation on rainfall. Geophys Res Lett 33:L09704. doi:10.1029/2005GL025155

Gonzalez PLM, Vera CS (2013) Summer precipitation variability over South America on long and short intraseasonal timescales. Clim Dyn. doi:10.1007/s00382-013-2023-2

Jones C, Waliser DE, Lau KM, Stern W (2004) Global occurrences of extreme precipitation events and the Madden–Julian oscillation: observations and predictability. J Clim 17:4575–4589

Jones C, Gottschalck J, Carvalho LMV, Higgins WR (2011) Influence of the Madden–Julian oscillation on forecasts of extreme precipitation in the contiguous United States. Mon Weather Rev 139:332–350

Kalnay E et al (1996) The NCEP/NCAR 40-year reanalysis project. Bull Am Meteorol Soc 77(3):437–471

Kidson JW (1999) Principal modes of Southern Hemisphere low-frequency variability obtained from NCEP-NCAR reanalyses. J Clim 12(9):2808–2830

Kiladis GN, Mo KC (1998) Interannual and intraseasonal variability in the Southern Hemisphere. In: Karoly DJ, Vincent DG (eds) Meteorology of the Southern Hemisphere. American Meteorological Society, Boston, MA, pp 307–336

Kiladis GN, Dias J, Straub KH, Wheeler MC, Tulich SN, Kikuchi K, Weickmann KM, Ventrice MJ (2014) A comparison of OLR and circulation-based indices for tracking the MJO. Mon Weather Rev 142:1697–1715

Lau WKM, Waliser DE (2012) Intraseasonal variability of the atmosphere–ocean climate system, 2nd edn. Springer, Heidelberg, p 613

Liebmann B, Allured D (2005) Daily precipitation grids for South America. Bull Am Meteorol Soc 86(11):1567–1570

Liebmann B, Kiladis GN, Marengo JA, Ambrizzi T, Glick JD (1999) Submonthly convective variability over South America and the South Atlantic convergence zone. J Clim 12:1877–1891

Liebmann B, Kiladis GN, Vera CS, Saulo AC, Carvalho LMV (2004) Subseasonal variations of rainfall in South America in the vicinity of the low-level jet east of the andes and comparison to those in the South Atlantic convergence zone. J Clim 17(19):3829–3842

Maharaj EA, Wheeler MC (2005) Forecasting an index of the Madden-oscillation. Int J Clim 25:1611–1618

Martin ER, Schumacher C (2011) Modulation of Caribbean precipitation by the Madden–Julian oscillation. J Clim 24:813–824

Mo KC, Higgins RW (1998) The Pacific-South American modes and tropical convection during the Southern Hemisphere winter. Mon Weather Rev 126(6):1581–1596

Muza MN, Carvalho LMV, Jones C, Liebmann B (2009) Intraseasonal and interannual variability of extreme dry and wet events over southeastern South America and the subtropical Atlantic during austral summer. J Clim 22(7):1682–1699

Naumann G, Vargas WM (2010) Joint diagnostic of the surface air temperature in southern South America and the Madden–Julian oscillation. Weather Forecast 25:1275–1280. doi:10.1175/2010WAF2222418.1

Nogues-Paegle J, Mo KC (1997) Alternating wet and dry conditions over South America during summer. Mon Weather Rev 125(2):279–291

Paegle JN, Byerle LA, Mo KC (2000) Intraseasonal modulation of South American summer precipitation. Mon Weather Rev 128:837–850

Pai DS, Bhate J, Sreejith OP, Hatwar HR (2009) Impact of MJO on the intraseasonal variation of summer monsoon rainfall over India. Clim Dyn. doi:10.1007/s00382-009-0634-4

Pohl B, Camberlin P (2006) Influence of the Madden–Julian oscillation on East African rainfall. I: intraseasonal variability and regional dependency. Q J R Meteorol Soc 132(621):2521–2539

Revell MJ, Kidson JW, Kiladis GN (2001) Interpreting low-frequency modes of Southern Hemisphere atmospheric variability as the rotational response to divergent forcing. Mon Weather Rev 129(9):2416–2425

Straub KH (2013) MJO initiation in the realtime multivariate MJO index. J Clim 26:1130–1151

Vera C et al (2006) Toward a unified view of the American monsoon systems. J Clim 19:4977–5000

Wheeler MC, Hendon HH (2004) An all-season real-time multivariate MJO index: development of an index for monitoring and prediction. Mon Weather Rev 132:1917–1932

Wheeler MC, Hendon HH, Cleland S, Meinke H, Donald A (2009) Impacts of the Madden–Julian oscillation on Australian rainfall and circulation. J Clim 22:1482–1498

Zhang L, Wang B, Zeng Q (2009) Impact of the Madden–Julian oscillation on summer rainfall in southeast China. J Clim. doi:10.1175/2008JCLI1959.1

Zhou Y, Thompson KR, Lu Y (2011) Mapping the relationship between Northern Hemisphere winter surface air temperature and the Madden–Julian oscillation. Mon Weather Rev 139(8):2439–2454

Zhou S, L'Heureux M, Weaver S, Kumar A (2012) A composite study of the MJO influence on the surface air temperature and precipitation over the continental United States. Clim Dyn 38:1459–1471